Precision Agriculture
https://doi.org/10.1007/s11119-022-09960-w

Improved estimation of herbaceous crop aboveground biomass using UAV-derived crop height combined with vegetation indices

Martina Corti[1] · Daniele Cavalli[1,2] · Giovanni Cabassi[2] · Luca Bechini[1] · Nicolò Pricca[2] · Dario Paolo[2,3] · Laura Marinoni[4] · Antonio Vigoni[5] · Luigi Degano[2] · Pietro Marino Gallina[1]

Accepted: 6 September 2022

Abstract
Vegetation indices are used in precision agriculture to estimate crop aboveground biomass (AGB) and, in turn, to quantify crop needs. However, crop species and development stage affect vegetation indices limiting the setup of generalized models for AGB estimation. Some approaches to overcome this issue have combined vegetation indices and structural crop properties such as crop height. However, only a few studies have considered different herbaceous crops like forages and cover crops. A 2-year field experiment was carried out on five winter cover crops with different habits at a high cover fraction (on average 93%) to study if combining vegetation indices, crop height and the fraction of soil covered by the crop could improve AGB estimation. Seven vegetation indices, crop height and cover fraction were derived from UAV-multispectral images. Species-specific and global (including all species) regression models were built and tested through cross-validation (CV). Green-based indices were the best estimators of AGB ($R_{CV}^2 = 0.56–0.93$, normalized root mean square error in CV nRMSECV = 26–38%) of the five species, separately. A global linear model using crop height alone, provided good results ($R_{CV}^2 = 0.57$, nRMSECV = 42%). Also, stepwise multiple regression was used to get a global model with crop height and five vegetation indices ($R_{CV}^2 = 0.75$, nRMSECV = 31%). Finally, a model was proposed where AGB was estimated by a vegetation index until plants covered 97% of soil or its height was shorter than 125 mm and by crop height for vegetation taller than 125 mm. The promising results ($R_{CV}^2 = 0.65$, nRMSECV = 36%) suggested the possibility of increasing AGB estimation by considering both vegetation indices and structural crop properties.

Keywords Crop surface models · Multispectral camera · Reflectance · Cover crops

✉ Martina Corti
martina.corti@unimi.it

Extended author information available on the last page of the article

Published online: 05 October 2022

Introduction

Since its first applications, remote sensing of vegetation has been used to characterize the type, amount and status of plants (Jackson & Huete, 1991). Such pieces of information have their main use in crop production especially in precision agriculture, where quick and spatialized detection of crop status is needed to guide site-specific crop management. Agricultural applications mainly involve the use of optical sensors able to record the relative amount of electromagnetic energy that is reflected or transmitted by the vegetation. This energy mainly gives information about leaf chlorophyll content (in the visible, red-edge regions) and leaf structural properties (in the near-infrared, NIR), that are linked to plant nutrient and water status, respectively (Corti et al., 2017). Spatialized reflectance data must be recorded quickly and on-demand to be satisfactorily used in operational conditions. Therefore, contactless multispectral sensors carried by tractors (such as CropCircle, Yara-N-sensor, GreenSeeker) and imaging sensors (multispectral cameras) airborne (often mounted on unmanned aerial vehicles, UAV) or satellite-mounted (Muñoz-Huerta et al., 2013) are the most used.

Measured reflectance values in the visible and NIR bands are linearly or non-linearly combined to calculate vegetation indices (Huete et al., 1997; Pinter et al., 2003). Since their first applications, vegetation indices have been shown to be affected by different factors such as the sensor type, background, atmospheric conditions, sensor view and solar angles (Jackson & Huete, 1991) but also by leaf color and canopy architecture (Pinter et al., 2003) that depend on crop species, variety and development stage and biotic and abiotic factors (Thenkabail et al., 2000). Different solutions were found to avoid negative effects of sensor's characteristics and external factors on the acquired spectra *e.g.,* setup of specific ambient conditions during spectra acquisition (Pauly, 2016; Rasmussen et al., 2016), the use of reference panel for radiometric calibration (Pauly, 2016), background noise removal (Noh et al., 2005), specific vegetation indices that mitigate background or atmospheric interferences (Mutanga & Skidmore, 2004). However, regardless of the type of vegetation index used and the crop species under study, both the saturation phenomenon (*i.e.,* vegetation indices reach their maximum values when the crop is still growing and therefore, at high vegetation cover fraction, vegetation indices underestimate crop biomass) and the effects of variety and development stage do not allow the development of empirical regression models estimating crop biophysical properties based on vegetation indices that are of general validity (Corti et al., 2018). They also could compromise other important applications of vegetation indices such as algorithms to support decision-making in site-specific crop management (Corti et al., 2020).

Some attempts to overcome saturation and specificity of vegetation indices were made by proposing new vegetation indices (Haboudane et al., 2002), by combining vegetation indices (Gu et al., 2013), or by proposing multivariate approaches that consider different wavelengths (Bendig et al., 2015). At the same time, advances in remote sensing led to the estimation of other variables more linked to crop structural properties such as crop height (Jimenez-Berni et al., 2018) and canopy volume (Calou et al., 2019), thanks to the development and the diffusion of new sensors such as LiDAR, multispectral imaging sensors for photogrammetry mounted on UAV, 3d reconstruction and ultrasonic sonars. Specifically, crop height is well known to be related to crop biomass within crop species (Madec et al., 2017) and final yield (Bendig et al., 2015). Moreover, it varies with variations of crop nitrogen and water availability (Azimi et al., 2021; Madec et al., 2017). For these reasons, the literature has focused on proving the ability of new sensors and on data analysis techniques

to provide good estimates of crop height; various sensors and techniques have been proposed and compared on different crops (Madec et al., 2017; Roth & Streit, 2018). Despite the great importance of crop height in describing crop status, only a few studies have verified the opportunity of integrating it with vegetation indices in order to improve the prediction of crop biomass (Sharma et al., 2016) using, specifically, plant height obtained from digital cameras mounted on UAVs. These studies adopted different approaches like the correction of vegetation indices by multiplication with crop height (Freeman et al., 2007) and the use of multiple regression models (Bendig et al., 2015). However, published works have focused on grain crops like cereals (Bendig et al., 2014; Freeman et al., 2007; Tilly et al., 2015), while herbaceous crops, cultivated for their leaves and stems (forage and cover crops), have rarely been the subject of these studies.

Therefore, the objective of this research was to verify if combining UAV-derived crop height with various commonly used vegetation indices could improve the estimation of aboveground biomass of herbaceous crop species having different plant habits, using data from a 2-year experiment on five forage and cover crop species.

Materials and methods

Experimental field

The study was carried out in an experimental field of 1.6 ha located in Sant'Angelo Lodigiano (Lodi), Italy, at Cascina Santa Martina of Morando Bolognini Foundation (45° 13′ 57.6″ N, 9° 25′ 36.7″ E, altitude 73 m asl), during 2017 and 2018 growing season. The field hosted an experiment on winter cover crops (Fig. 1) aimed at studying the effects of crop species, date of sowing and maize post-harvest soil mineral nitrogen on aboveground biomass production and nitrogen removal of cover crops and cover crops competition with weeds. The experimental factors were crop species, date of sowing and post-harvest soil

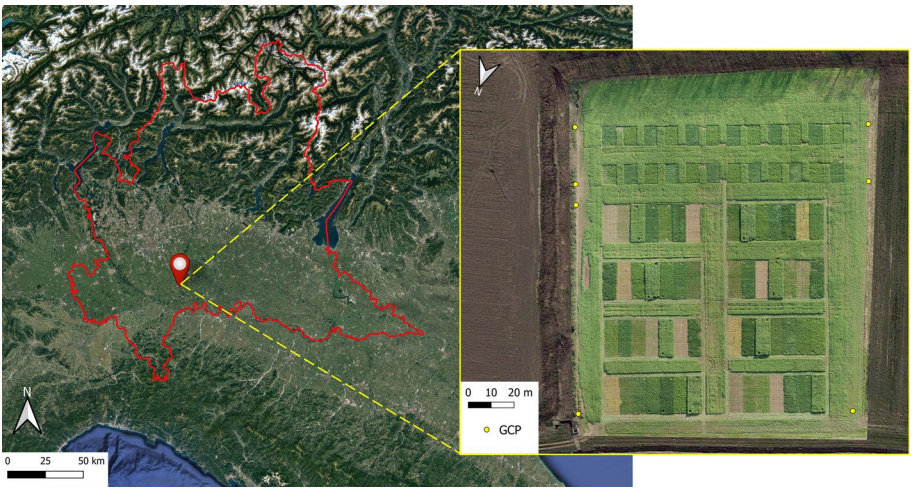

Fig. 1 Experimental site in Lombardy and focus on the ortho-image of the experimental field captured by a Sony a6000 camera in October 2017. Yellow dots represent the positions of the seven ground control points (GCP)

mineral nitrogen. Five cover crops species were compared: two grasses, *Avena strigosa* Schreb. Saia variety (black oat, OAT) and *Secale cereale* L. Stanko variety (rye, RYE); two legumes, *Vicia villosa* Roth Villana variety (hairy vetch, HVE) and *Trifolium alexandrinum* L. Mario variety (Egyptian clover, CLO); and a cruciferous, *Sinapis alba* L. Architect variety (white mustard, WMU). In addition, weeded and non-weeded control treatments were included. Two sowing dates (6th and 22nd September of both 2017 and 2018) and two application rates of nitrogen were tested: 0 kg N ha^{-1}; and 50 kg N ha^{-1} $year^{-1}$ as calcium nitrate applied before sowing the cover crops. The experimental factors were combined according to a complete factorial design with four replicates (blocks) arranged in a hierarchical split-split plot design with sub-sub plots of 48 m^2 each (6×8 m). The field experiment provided a large dataset (N = 240, as a result of the factorial combination of 5 species × 2 sowing dates × 2 soil N × 4 replicates × 3 campaigns of crop samplings), characterized by great variability in aboveground biomass generated by the combination of the experimental factors and great variability of the five crop habits.

Figure 2 shows images with front and top views of the plots to give an example of the different plant architectures and soil coverage of the tested cover crops.

The soil of the field was flat and with homogeneous properties and characterized by 45% sand, 41% silt and 14% clay, by the absence of skeleton, by sub-acid reaction (pH $H_2O = 6.0$) and 1.5% organic matter. The climate of Sant'Angelo Lodigiano is characterized by annual average precipitation of 830 mm and an average temperature of 13.2° C. During the year 2017, on 10th October, irrigation was done in order to prevent water stress due to scarce precipitation in that period.

Aerial surveys

Aerial surveys of the field were made at three different dates in order to be able to monitor the highest levels of cover crop growth: 30th October 2017, 20th November 2017 and 18th November 2018. A handmade coaxial octocopter, with a maximum takeoff mass of 12 kg and equipped with a GNSS (global navigation satellite system) NEOM8N (ublox, Thalwil, Switzerland) and a gimbal platform-mounted multispectral MicaSense Red-edge

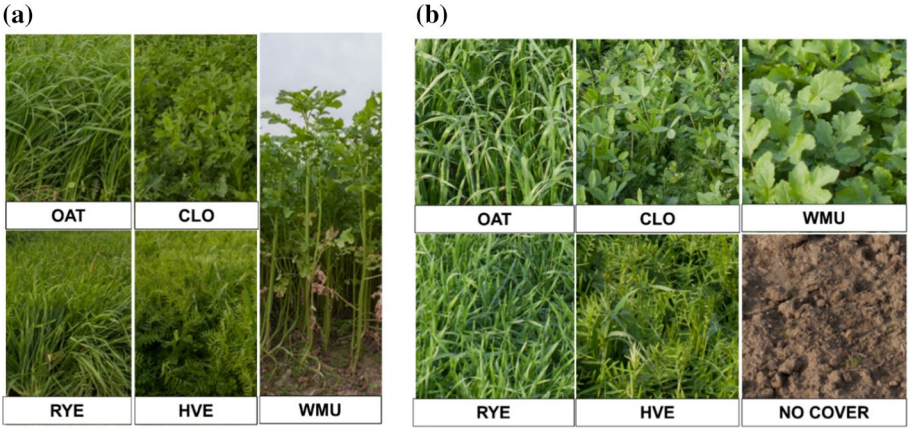

Fig. 2 Front **a** and top **b** views of the cover crops: black oat, OAT; rye, RYE; hairy vetch, HVE; Egyptian clover, CLO; and white mustard, WMU

camera (sensor resolution: 1.2 MP per band; MicaSense, Inc., Seattle, WA, USA) which is a professional digital camera for agriculture applications. It acquires reflectance in a blue band (475 ± 20 nm; a green band (560 ± 20 nm); a red band (668 ± 10 nm); a red-edge band (717 ± 10 nm); a near-infrared band (840 ± 40 nm). The images of a white reference panel (Spectralon®) were acquired before and after each flight in order to perform radiometric calibration of the images. Nadir images of the fields were collected at an altitude of 60 m, at solar noon, with a clear sky. The solar elevation angles were low ranging from 24° for the surveys made in November to 29° for the October 2017 survey, while solar Azimuth varied between 192° and 194°, respectively. The flight plan guaranteed 85% of forward and sideward overlap, needed for image processing.

Photogrammetry and image processing

Pix4Dmapper software (version 4.3.33; Pix4D SA, Lausanne, Switzerland) was used to build the ortho-mosaics and the crop surface models (CSMs) of the experimental field. The ortho-mosaics of the five bands recorded were built to calculate the maps of vegetation indices; the CSMs were built in order to estimate crop height. Specifically, CSM is a raster file that represents the Earth's surface including objects on it (*i.e.,* crop plants) and it was built with the following settings of Pix4Dmapper software: noise filtering and surface smoothing were applied on the points cloud and the triangulation method was used to produce the raster files. The outputs of the processed images consisted of five different reflectance TIFF images (16bit grayscale per band) and one crop surface model (TIFF file) for each field survey. Ortho-images and CSMs had a spatial resolution of 40 mm.

The GNSS position (precision 0.012 m) of seven artificial targets (ground control points taken with the Topcon GRS-1 GNSS RTK Receiver; TopCon Corporation, Tokyo, Japan) was used for geometric correction (Fig. 1). Finally, the software QGIS (version 3.10; QGIS.org, 2020) was used to calculate UAV-based variables *i.e.,* estimated crop height, vegetation indices and vegetation cover fraction. These variables were extracted, for each sampling date, by sampling in each ortho-image and CSM, from a 1 m^2 area (as polygonal shapefile) positioned in the center of each plot.

Structural crop properties: estimation of UAV-derived crop height and vegetation cover fraction

Crop height was estimated (Hest) from CSMs. Since the CSM measures the altitude of Earth plus the crop on its surface, Hest was calculated as the difference between the altitude of the crop (calculated as the 95° percentile of the altitude of each plot and bare soil). The altitude of the bare soil was retrieved by sampling the CSM of chemically weeded plots, used as reference of bare soil. Within each sampling campaign, a single reference soil altitude was used for the whole field and was set to the mean of all bare soil plots (n = 16, corresponding to treatments without cover crops, uniformly spread on the experimental field; Fig. 2). The altitude of bare soil was checked in every CSM and it showed random differences (< 150 mm) indicating a flat field, characterized by the absence of a soil slope across plots. Moreover, soil compaction in non-weeded control plots was the same as that in crop plots because all agronomic operations potentially causing soil compaction (including seeding) were applied on cropped and control plots.

The vegetation cover fraction (FC) of the crops was calculated in every plot of each ortho-image. A threshold was established on the red-edge band by using the function

graythresh that implemented the Otsu algorithm (Otsu, 1975) in MATLAB software (version 2014b, the Mathworks, Inc., MA, USA). The procedure provided a binary image separating plants from their background, by producing a black and white image where white pixels belong to vegetation and black pixels are the pixels of soil. Then, the FC was calculated for each plot as the ratio between the number of white pixels and the total number of pixels in the plot.

UAV-derived vegetation indices

Seven vegetation indices were calculated for each plot: two red-based indices, the normalized difference vegetation index (NDVI) and the optimized soil adjusted vegetation index (OSAVI); two green-based indices, the green normalized difference vegetation index (GNDVI) and the chlorophyll green index (CIg); two red-edge-based indices, the normalized difference red-edge index (NDREI) and the chlorophyll red-edge index (CIre); and one multiple-band vegetation index, the triangular vegetation index (TVI). These indices were chosen because they had been already tested in the literature for AGB estimation under high soil coverage on the species tested in this study or similar (Table 1).

Ground measurements

At the same dates as UAV field surveys, reference ground measurements of AGB and crop height were taken. Plants of cover crops and weeds (if any) were harvested from 1 m^2 representative of each plot. Cover crops and weeds were separated and weighed to collect their fresh weight. Then, a sub-sample was oven-dried (105 °C) until constant weight in order to obtain AGB values on a dry weight (DW) basis of both cover crops and weeds. On the same day, the average height of plants on 1 m^2 was recorded using a graduated stick (precision 0.01 m) and a spirit level. Three measurements per plot were taken close to the AGB sampling area and they were averaged.

Data analysis

Data analysis was carried out using the R software (version 3.6.2; R Core Team, 2019). Descriptive statistics of measured and UAV-based crop variables were calculated using *describe* and *describeBY* functions of the "psych" R package (version 2.0.9; Revelle, 2020). Scatterplots were made using the "ggplot2" R Package (version 3.3.5, Wickham, 2016).

Table 1 Vegetation indices tested in this study

Vegetation index	Equation
NDVI	(NIR – R)/(NIR + R)
OSAVI	(1 + 0.16)(NIR – R)/(NIR + R + 0.16)
GNDVI	(NIR – G)/(NIR + G)
CIg	(NIR/G) – 1
NDREI	(RE – R)/(RE + R)
CIre	(NIR/RE) – 1
TVI	0.5[(120(NIR – G) – 200(R – G))]

B, G, R, RE and NIR are the blue, green, red, red-edge and near-infrared bands recorded by the multispectral camera (MicaSense Red-edge)

Firstly, a simple regression model was built between ground-measured and UAV-derived crop height in order to test the quality of the UAV estimation and to calculate the limit of quantification (LOQ). The LOQ identifies the smallest ground-measured crop height that can be quantitatively detected by the UAV. It is defined in Eq. 1 (Shrivastava & Gupta, 2011).

$$LOQ = 10\frac{Sy}{m} \tag{1}$$

where Sy is the standard deviation of y-intercept and m is the slope of the linear regression model between UAV-based crop height and ground-measured crop height. The bias of UAV-derived crop height was also calculated as the difference between the mean of estimates and the true value of the variable being estimated.

Then, simple regression models were fitted using *lm* function of the "R stats" package (version 3.6.2; R Core Team, 2019) to predict AGB from different predictors Hest, vegetation indices and FC: linear fit, exponential fit and polynomial fits were tested. In addition, a multiple regression model was built to combine the seven vegetation indices, Hest and FC in one global calibration model, fitted for all species together. For this purpose, backward stepwise linear regression was carried out using the "leaps" R package (version 3.1; Lumley, 2020).

Another regression method was adopted. It consisted of combining two regression models with the following rules:

$$\text{AGB} = \text{f(VI) if FC} < \text{ FCsat or Hest} \leq \text{LOQ} \tag{2}$$

$$\text{AGB} = \text{ f(Hest) if FC} \geq \text{FCsat and Hest} \geq \text{LOQ} \tag{3}$$

where f(…) indicates the global calibration model with the best fit for the given predictor. The FCsat is the saturation of the vegetation cover fraction and it was defined by fitting a segmented linear regression model between FC and AGB and finding the break-point (plateau). The "segmented" R package (version 1.3–4; Muggeo, 2008) was used. At first, the whole dataset (all species together) was divided into two parts accordingly to the values of the FCsat and LOQ of Hest (Eq. 1). Then, global calibration curves for each vegetation index (VI) were fitted separately and the best regression model (either linear, exponential, or polynomial) was selected to estimate AGB from VI until FCsat occurs (Eq. 2), or if Hest is lower than the LOQ. Above saturation (Eq. 3), AGB was estimated from a global calibration curve with Hest, only if it is greater than the LOQ.

Statistics of the performances of regression models

The simple and multiple regression models were tested by the contiguous block cross-validation using the "caret" R package (version 6.0–90; Kuhn, 2021). The setting of cross-validation was planned considering that the original experiment was arranged in four blocks of replicates. Therefore, four folds were produced so that at every cancellation step, one block was used as the test set. Since the dataset was composed of three dates of sampling in a 2-year experiment, all the observations of all the years belonging to the same block were left out per cancellation group. The resulting sample size in cross-validation were: 36 samples in the training set and 12 samples in the test set for the species-specific regression models, 180 samples in the training set and 60 samples in the test set for the calibration of global models.

The determination coefficients in cross-validation (R_{CV}^2), the root mean square error in cross-validation (RMSECV), the normalized root mean square error in cross-validation (nRMSECV, represented by the RMSECV divided by the mean of the observed variable) and the mean absolute error in cross-validation (MAECV) of the fitted regression models were calculated.

Results

Variability of the reference dataset

Table 2 shows the descriptive statistics of the ground-based measurements. The statistics of UAV-derived predictors are shown in Table S1 of the supplementary material.

For CLO and HVE, in most cases, plants were small with the lowest AGB levels (Table 2), resulting in the lowest NIR reflectance values (data not shown). The highest AGB and FC were reached by OAT and WMU (Table 2; Table S1). Rye plants had high AGB levels but lower crop height. In general, the distributions of FC values showed a negative skewed distribution for all cover crop species (Table S1), indicating a higher frequency of high compared to low FC values and thus suggesting that saturating levels were reached. Descriptive statistics of the vegetation indices and crop heights (both ground-measured and UAV-based) demonstrated their high variability, adequate for calibration purposes (Table 2; Table S1).

Table 2 Descriptive statistics (mean ± standard deviation (StD), minimum (Min), maximum (Max) and skewness) of the ground-measured variables on three dates together (30th October 2017; 20th November 2017; 18th November 2018): aboveground biomass (AGB), total and of weeds alone, crop height

Crop variable	Crop species	Mean ± StD	Min	Max	Skewness
Total AGB (g DW m^{-2})	CLO	109.3 ± 101.9	9.0	345.3	0.83
	HVE	152.6 ± 100.2	20.2	376.3	0.58
	OAT	174.0 ± 78.0	58.3	344.6	0.40
	RYE	178.2 ± 63.1	69.8	323.9	0.27
	WMU	261.0 ± 125.5	75.8	603.5	0.83
Weeds AGB (g DW m^{-2})	CLO	41.5 ± 66.3	0.0	282.1	1.75
	HVE	33.6 ± 60.7	0.0	283.2	2.75
	OAT	10.4 ± 16.9	0.0	56.3	1.41
	RYE	2.6 ± 7.2	0.0	28.5	2.69
	WMU	0.1 ± 0.9	0.0	6.1	6.50
Ground-measured crop height (mm)	CLO	21.4 ± 14.9	4.0	50.0	0.47
	HVE	208 ± 120	53	457	0.58
	OAT	429 ± 120	250	700	0.67
	RYE	222 ± 65	90	347	− 0.21
	WMU	721 ± 244	290	1270	0.26

UAV-derived crop height

Ground-measured crop height was successfully estimated by UAV-derived crop height (Hest). The two measurements were linearly correlated with an R^2 of 0.8 (Fig. S1). The LOQ was also estimated by Eq. 1 and it resulted in 125 mm. It means that under that threshold, the UAV-crop height could not be quantified correctly. Eighteen percent of the entire dataset had a crop height under the LOQ. However, Hest bias was 88 mm, lower than the LOQ. This results confirmed that Hest was successfully derived by the UAV survey with the multispectral camera using the CSM method. It must be noted that the height of smaller plants could have been be affected by the use of one altitude value of the bare soil for the entire field.

Simple regression models for AGB estimation

UAV-derived crop variables, either vegetation indices or structural properties, were tested for the estimation of AGB. Scatterplots of AGB *vs.* each predictor are shown in Fig. 3. Scatterplots of data divided by predictor and cover crop species are visible in Fig. S2 of the supplementary material.

Vegetation indices as AGB predictors

The best fits of simple regression models between AGB and vegetation indices were exponential and polynomial (Table 3). The statistics of all the models tested are visible in Table S2 of the supplementary material. The MAECV was much lesser than RMSECV for all crop species and calibration curves indicating overall acceptable errors. Nonetheless, nRMSECV was commented in the main text for simpler comparisons among the species-specific calibration curves.

The green-based vegetation indices (CIg and GNDVI) had the best performance in the estimation of the AGB of all the species with R_{CV}^2 of the exponential models varying from 0.56 to 0.93 and nRMSECV from 26 to 38% and MAECV from 25 to 67 g DW m^{-2} (Table 3). The GNDVI was the best index to predict AGB of CLO and RYE (R_{CV}^2 of 0.93 and 0.61, respectively), while CIg was the best predictor for HVE, OAT and WMU with R_{CV}^2 of 0.85, 0.59 and 0.57, respectively. The vegetation indices showing the highest errors (nRMSECV from 35 to 88% and MAECV from 51 to 95 g DW m^{-2}) were those based on the red-edge (CIre and NDRE). Moreover, the CIre and NDRE showed a dependence on crop species and development stage, separating October 2017 and November 2018 (autumn 2018 had low precipitation with less developed plants) from November 2017 (Fig. 3). The OSAVI, TVI and NDREI showed dependence on the timing of the survey and/or FC. Specifically, they clearly separated the early sampling date from the late sampling *i.e.,* October 2017 *vs* November 2017 and November 2018. Finally, the NDVI had similar behavior and nRMSECV to the OSAVI, TVI and NDREI, with errors from 31 to 55%. Finally, NDVI, OSAVI, NDREI and GNDVI showed a saturating behavior.

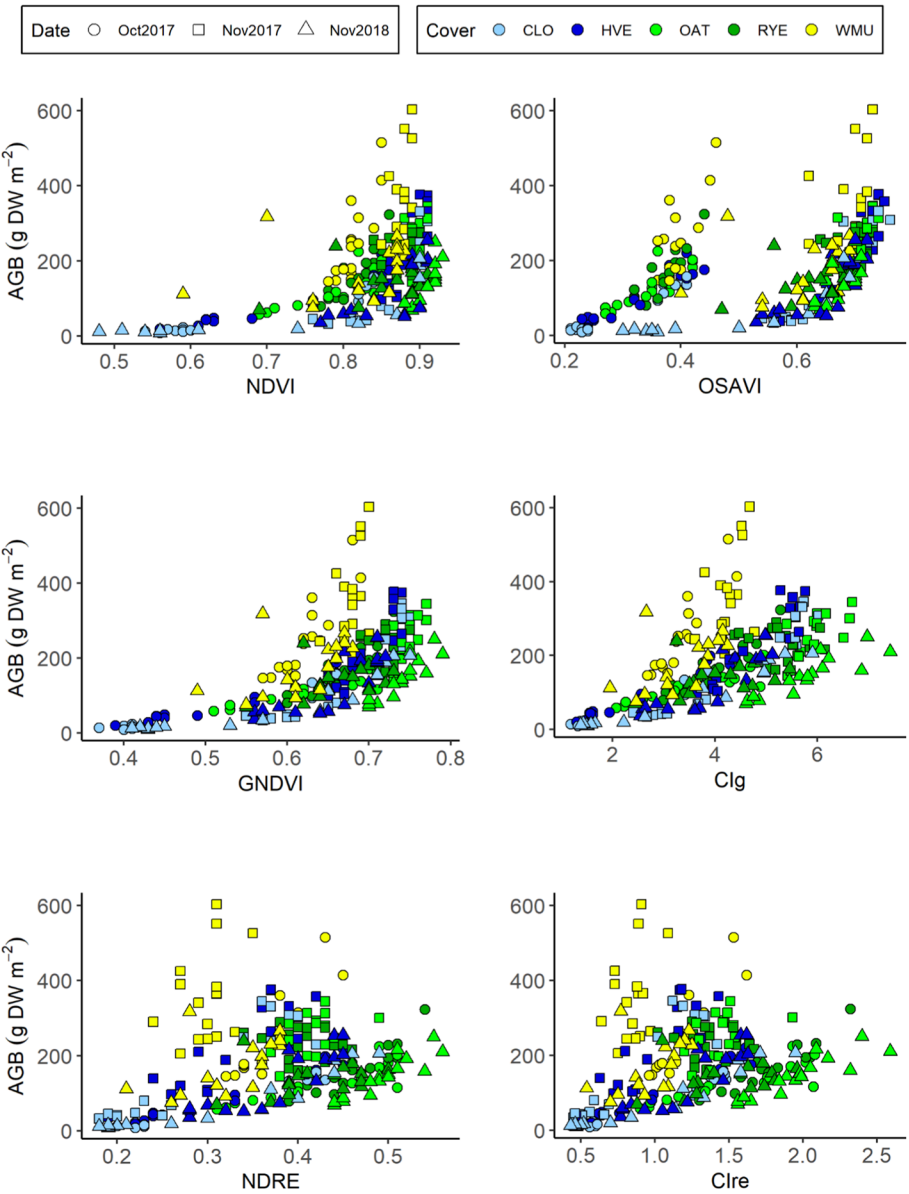

Fig. 3 Scatterplots of UAV-derived variables and aboveground biomass (AGB). Crop species and sampling dates have different colors and shapes, respectively. For the abbreviations of crop species, see the caption of Fig. 2

UAV-derived crop height and vegetation cover fraction as AGB predictors

Due to the robustness of Hest and FC (structural variables) regardless of crop species, development stage and timing of the survey (Fig. 3), it was possible to develop

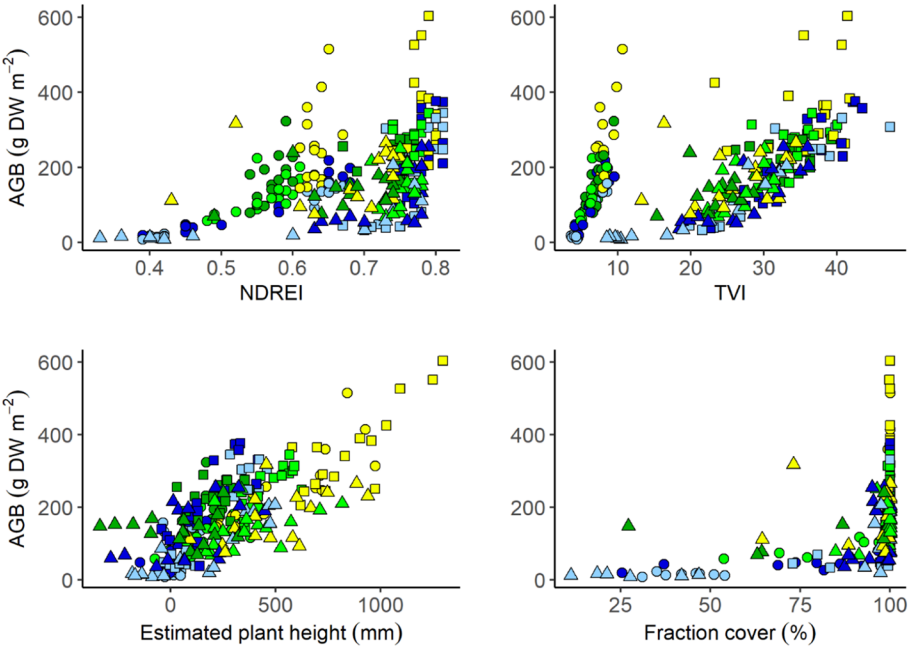

Fig. 3 (continued)

crop-specific and global *(i.e.,* including all cover crops) calibration models, by fitting simple regression models on the entire dataset including all species (Table 4).

For WMU, crop Hest was a better estimator of AGB compared to FC and the best vegetation index (CIg), with R_{CV}^2 of 0.72, nRMSECV of 28% and the lowest MAECV (Table 4). The AGB of OAT was also estimated well using Hest, with performance very similar to the ones of the best vegetation index (Table 3): R_{CV}^2 of 0.58 and nRMSECV of 35% even with a slightly higher MAECV (Table 4). Good results were obtained by the global calibration model: the best fit was linear with R_{CV}^2 of 0.57 and nRMSECV of 42%. Finally, a global calibration was also possible for the FC (Table 4). Nonetheless, it showed a clear saturating behavior with a plateau at 97.2%, corresponding to 99.7 g DW m^{-2} (Fig. 3).

Multiple regression models for AGB estimation

The calibration of the global regression models was carried out with the aim of proposing a unique equation for the estimation of AGB of various herbaceous crop species. The best multiple regression model obtained via backward stepwise regression (Fig. 4a) was better than the simple model based on Hest alone (Table 4) and showed predictive ability comparable to the models based on single vegetation indices applied to the species separately (Table 3). The model included six predictors: Hest and five vegetation indices. The GNDVI was selected instead of CIg probably because it better explained the variability of the AGB of RYE that was not properly estimated by other vegetation indices (Table 3). Moreover, the OSAVI, TVI and NDREI, all affected by the timing of the survey and/or FC, were

Table 3 Simple regression models for the estimation of aboveground biomass (AGB) of the different cover crop species from vegetation indices of all dates

Predictor	Crop	Best fit	Fitted model for AGB estimation (g DW m^{-2})	R_{CV}^2	RMSECV (g DW m^{-2})	nRMSECV (%)	MAECV (g DW m^{-2})
NDVI	CLO	Exponential	$0.2*e^{7.6*x}$	0.85	60.2	55	41.2
	HVE	Exponential	$0.6*e^{6.5*x}$	0.66	68.9	45	50.5
	OAT	Exponential	$2.7*e^{4.7*x}$	0.38	67.0	38	52.2
	RYE	Exponential	$3.0*e^{4.7*x}$	0.35	55.2	31	44.9
	WMU	Exponential	$6.3*e^{4.3*x}$	0.35	111.8	43	84.3
OSAVI	CLO	Polynomial	$1309.7*x^2-872.9*x+174.86$	0.60	64.2	59	53.8
	HVE	Polynomial	$1244.4*x^2-893.0*x+226.3$	0.44	75.9	50	63.8
	OAT	Exponential	$59.6*e^{1.7*x}$	0.39	63.7	37	51.8
	RYE	Exponential	$95.6*e^{*x}$	0.19	58.7	33	48.7
	WMU	Polynomial	$3891.8*x^2-3963.7*x+1183.9$	0.19	114.2	44	90.7
GNDVI	**CLO***	**Exponential**	$0.3*e^{8.9*x}$	**0.93**	**35.9**	**33**	**25.1**
	HVE	Polynomial	$4810.5*x^2-4790.7*x+1212.2$	0.82	45.5	30	37.7
	OAT	Exponential	$4.0*e^{5.2*x}$	0.56	56.3	32	44.3
	RYE	**Exponential**	$2.7*e^{6.0*x}$	**0.61**	**45.9**	**26**	**35.2**
	WMU	Exponential	$1.7*e^{7.7*x}$	0.56	90.8	35	68.7
CIg	CLO	Exponential	$5.8*e^{0.7*x}$	0.93	41.4	38	24.4
	HVE	**Exponential**	$14.6*e^{0.6*x}$	**0.85**	**40.7**	**27**	**32.6**
	OAT	**Exponential**	$38.0*e^{0.3*x}$	**0.59**	**55.8**	**32**	**44.8**
	RYE	Exponential	$44.5*e^{0.3*x}$	0.56	48.0	27	37.5
	WMU	**Exponential**	$32.2*e^{0.5*x}$	**0.57**	**87.6**	**34**	**67.3**
NDRE	CLO	Exponential	$2.7*e^{10.1*x}$	0.74	79.1	72	50.5
	HVE	Exponential	$8.3*e^{7.7*x}$	0.58	81.1	53	58.3
	OAT	Exponential	$50.0*e^{2.6*x}$	0.10	78.3	45	61.9
	RYE	Exponential	$84.0*e^{1.6*x}$	0.05	62.9	35	50.8
	WMU	Exponential	$112.7*e^{2.2*x}$	0.09	125.2	48	95.3
CIre	CLO	Exponential	$7.3*e^{2.2*x}$	0.71	95.7	88	57.2
	HVE	Exponential	$20.1*e^{1.6*x}$	0.55	84.5	55	60.7
	OAT	Exponential	$85.6*e^{0.4*x}$	0.09	78.5	45	62.1
	RYE	Exponential	$110.9*e^{0.3*x}$	0.06	62.6	35	50.6
	WMU	Polynomial	$373.9*x^2-692.4*x+560.7$	0.11	121.5	47	91.4
NDREI	CLO	Exponential	$1.1*e^{6.3*x}$	0.74	68.9	63	52.4
	HVE	Exponential	$4.2*e^{4.8*x}$	0.54	75.7	50	59.9
	OAT	Exponential	$23.5*e^{2.7*x}$	0.36	66.3	38	53.6
	RYE	Exponential	$67.4*e^{1.3*x}$	0.26	56.9	32	47.0
	WMU	Exponential	$44.0*e^{2.4*x}$	0.21	116.5	45	87.0
TVI	CLO	Polynomial	$0.3*x^2-5.1*x+70.8$	0.69	57.5	53	48.2
	HVE	Polynomial	$0.3*x^2-10.2*x+143.0$	0.63	61.4	40	53.1
	OAT	Polynomial	$0.3*x^2-8.8*x+162.6$	0.60	53.2	31	44.9
	RYE	Polynomial	$0.3*x^2-8.4*x+203.7$	0.33	53.3	30	44.1
	WMU	Polynomial	$0.5*x^2-20.6*x+378.6$	0.29	107.5	41	83.1

The table reports the equation of the best fit for each combination of index and crop species, the coefficient of determination in cross-validation (R_{CV}^2), the root mean square error in cross-validation (RMSECV), the normalized root mean square error in cross-validation (nRMSECV) and the mean absolute error (MAECV) are reported. For the abbreviations of crop species, see the caption of Fig. 2

Table 3 (continued)

*The vegetation index with the best fit is in bold

Table 4 Simple regression models for the estimation of aboveground biomass (AGB) from structural predictors of all dates for different cover crop species and for the global dataset including all species

Predictor	Crop	Best fit	Fitted model for AGB estimation (g DW m^{-2})	R_{CV}^2	RMSECV (g DW m^{-2})	nRMSECV (%)	MAECV (g DW m^{-2})
Hest (mm)	CLO	Linear	$0.4*x+53.0$	0.77	65.0	59	52.0
	HVE	Polynomial	$0.0003*x^2+0.4*x+97.9$	0.60	71.1	47	59.6
	OAT	Exponential	$84.5*e^{0.002*x}$	0.58	61.2	35	48.4
	RYE	Linear	$0.2*x+154.9$	0.25	61.5	35	53.1
	WMU	Polynomial	$0.0002*x^2+0.03*x+124.5$	0.72	73.0	28	55.8
	Global	Linear	$0.3*x+98.4$	0.57	72.7	42	59.9
FC (%)	CLO	Exponential	$4.4*e^{0.03*x}$	0.72	79.9	73	53.2
	HVE	Exponential	$5.6*e^{0.03*x}$	0.51	88.7	58	68.9
	OAT	Exponential	$7.4*e^{0.03*x}$	0.40	69.2	40	55.4
	RYE	Exponential	$64.7*e^{0.01*x}$	0.26	60.3	34	49.8
	WMU	Exponential	$42.8*e^{0.02*x}$	0.30	124.8	48	92.3
	Global	Exponential	$5.4*e^{0.03*x}$	0.54	94.7	54	68.2

The table reports the equation of the best fit for each species, the coefficient of determination in cross-validation (R_{CV}^2), the root mean square error in cross-validation (RMSECV), the normalized root mean square error in cross-validation (nRMSECV) and the mean absolute error (MAECV). For the abbreviations of crop species, see the caption of Fig. 2

selected as well as CIre that strongly depended on crop species and development stage (Fig. 3).

The approach of using the best predictor among vegetation indices together with Hest was also tested in order to propose a simpler method able to account for the vegetation indices and structural crop properties by considering the limit of the saturation of FC and the LOQ of the Hest (125 mm). The CIg was chosen due to its good performances in the estimation of AGB of single species (Table 3) and because of its linear correlation with AGB of the global dataset. The proposed model (Fig. 4b), compared to the multiple regression model, had only a slight worsening of the R_{CV}^2 and errors, of 10% and 5%, respectively, but with the use of only three predictors (CIg and Hest; plus FC to define saturation) against the six predictors of the multiple regression model.

Discussion

The main objective of this study was to test the combination of vegetation indices and crop structural properties to estimate the AGB of different species of crops at high levels of vegetation cover fraction.

Field campaigns were scheduled to guarantee the sampling of AGB at the highest levels of cover crop production. In fact, even if past works on AGB estimation from vegetation indices identified the saturation issue, authors did not identify and report absolute AGB

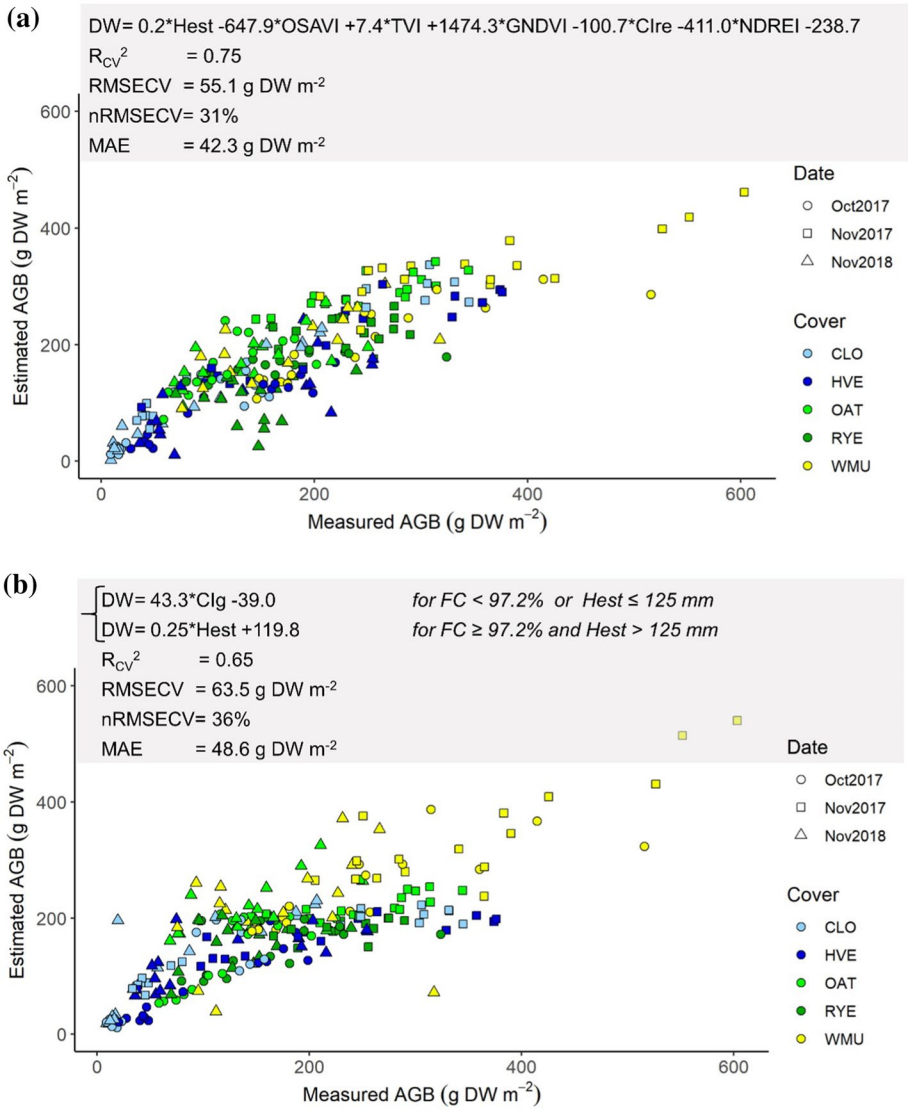

Fig. 4 Measured *vs.* estimated crop above-ground biomass (AGB) by multiple regression model (**a**) and by a combination of regression models (**b**)

values that caused the saturation of vegetation indices (Gu et al., 2013; Huete et al., 1997; Mutanga & Skidmore, 2004; Poley & McDermid, 2020). The measured crop FC confirmed that saturation was reached at 97.2% of FC at 99.7 g DW m^{-2} of AGB, considering all crops together.

However, vegetation indices showed different behavior with respect to FC suggesting that they were influenced by different factors other than AGB such as leaf color, plant architecture and development and the timing of the survey. In agreement with the literature, the NDVI was the most affected by saturation (Gu et al., 2013; Huete et al., 1997; Mutanga

& Skidmore, 2004). It saturated following the same behavior of the FC, confirming the strict connection of NDVI with it. Among the tested vegetation indices, the best results were reached by the green-based vegetation indices (Table 3). The indices based on the red-edge band, CIre and NDRE, showed low correlations with AGB, probably due to the effect of different development stages included in the models (Fig. 3, Table 3), in contrast with results of other similar works (Mutanga & Skidmore, 2004; Wang et al., 2016). Finally, OSAVI, TVI and, in small part, NDREI, used to limit soil effects on crop reflectance, showed a dependence on the timing of data acquisition (Fig. 3), contrary to previous studies (Huete et al., 1997; Prabhakara et al., 2015). However, the index OSAVI was designed to overcome the noise of soil brightness (Goel & Qin, 1994) and the TVI was designed to be more sensitive to chlorophyll content and to be less affected by atmospheric conditions (Vincini et al., 2006). These corrections could have caused the indices' values to be different in early autumn (October 2017) with respect to the values of the same indices measured in November in both years, considering the presence of smaller plants and the higher solar elevation angle of the sun in October. For these reasons, it must be considered that an accurate atmospheric correction of UAV-derived images could lead to better results (Cao et al., 2020).

As opposed to vegetation indices, crop height was strongly related to crop growth and it was not dependent on other factors. It was evident by the linear relationship between crop height and AGB with no deviations due to development stage, sampling date or species (Fig. 3). Therefore, it allowed the calibration of a global model for the estimation of AGB according to attempts already reported in the literature (Roth & Streit, 2018). The best fit resulted in a linear regression model that proved the consistency of the correlation between crop height and AGB with no saturation even at high AGB levels. Despite some issues that could arise when estimating AGB at early stages with low crop heights, the good results obtained confirmed the interest in crop height as a rough powerful estimator of AGB irrespective of crop species. With these premises, global calibration models were also tested using all the UAV-derived variables in order to overcome the specificity of AGB estimation by vegetation indices. As expected, the multiple regression model led to the best results in AGB estimation (Fig. 4a). Both UAV-derived crop height and five vegetation indices were selected by the model, indicating that the combination of vegetation indices and structural crop properties improved the estimation of AGB. Similar results were obtained in previous studies that tested the ability of multiple linear and non-linear regression models using crop height and vegetation indices to estimate AGB of cereal crops (Bendig et al., 2014, 2015; Marshall & Thenkabail, 2015; Tilly et al., 2015). The vegetation indices selected by the backward procedure of the multiple regression model were those affected by crop species and/or development stage (CIre) or FC and/or timing of the survey (TVI, OSAVI and NDREI), other than GNDVI, that, with CIg, was the best index to predict AGB. This result pointed out the need for predictors that accounted for the difference among species and development stages in order to explain the variability of the collected dataset. However, according to the literature, it was observed that, when plants are very small with dense canopies, vegetation indices (specifically, the green-based indices) are very sensitive to differences in crop growth and are suitable for the estimation of AGB (Roth & Streit, 2018; Tilly et al., 2015). Otherwise, when plants have a vertical growth and FC is saturated, crop height is the best estimator of AGB. For the abovementioned reasons, a new regression approach was proposed for the first time in this study (Fig. 4b). It combined two predictors: the best vegetation index (in terms of AGB prediction) was used to predict AGB until FC saturation occurred or when the Hest was under the estimated LOQ. Otherwise, Hest was used. The proposed method overcomes the saturation phenomenon by using vegetation

indices at low FC levels when they have the power to detect small changes in soil coverage and use Hest when it is maximally related to AGB when FC is high and vegetation indices lose their ability to detect changes in AGB, also caused by crop vertical growth. Moreover, the use of different regression models for different predictors overcame the overfitting that could have affected the multiple regression model that was applied on correlated predictors, in this case the vegetation indices (r = 0.10–0.97, Table S3).

In this context, the results were very promising. Statistics in cross-validation showed a small decrease with respect to the multiple regression model (Fig. 4) if compared to the decrease in the number of predictors (two uncorrelated *vs.* six correlated, respectively). Moreover, the results were comparable to the performance of regression models of studies that proposed multiple regression approaches on only one crop species (Bendig et al., 2014, 2015; Marshall & Thenkabail, 2015; Tilly et al., 2015) confirming the possibility of overcoming the specificity of vegetation indices in the estimation of AGB and producing advancement with respect to previous works on similar herbaceous crops that did not explore the combination of the vegetation indices and structural crop properties for the estimation of AGB (Roth & Streit, 2018).

Future perspectives

As a result of this work, two crucial aspects for the improvement of the estimation of herbaceous crop AGB emerged. Firstly, a larger dataset with more variability in the initial crop growth stages and different plant habits is fundamental to extend the proposed calibration models and to prove the robustness of the proposed approaches. Secondly, different ways to estimate crop height also at early crop development stages should be studied with different sensors on crops with different plant habits to retrieve reliable crop height estimates in operational conditions. In fact, this study confirmed that plant height can be successfully estimated by UAV-derived CSMs (Poley & McDermid, 2020; Roth & Streit, 2018). However, crop height estimation from airborne images should be improved. Specifically, these results showed that the LOQ of the estimation of crop height was 125 mm. Moreover, it must be considered that an average altitude of the field was used to estimate crop heights, so the height and AGB of small plants with horizontal habits were difficult to quantify. To gain even better results, more accurate methods of estimating plant height should be considered *e.g.,* having reference altitudes measured in the fields (more than 30 points) to build digital terrain models or making an aerial survey of the bare soil of the field. Finally, different technologies should be considered such as LiDAR (Deery et al., 2014; Wiering et al., 2019) or ultrasonic sensors mounted on tractors (Farooque et al., 2013) as well as more resolved imaging sensors such as RGB cameras with very high spatial resolutions.

Conclusions

The estimation of herbaceous crop aboveground biomass was tested using both vegetation indices and structural crop properties. It was estimated by green-based vegetation indices with varying degrees of success for the different crop species ($R_{CV}^2 = 0.56–0.93$, nRMSECV = 26–38%). Also, plant height was a good estimator of aboveground biomass with a more linear correlation to it. Consequently, at first, crop height was used for the calibration of a global model for AGB estimation of all species together, regardless of the development stage, the timing of the survey and vegetation cover fraction, with good results

($R_{CV}^2 = 0.57$, nRMSECV = 42%). Even if with slightly worse performance, a global curve for aboveground biomass estimation is more interesting for simplicity and possibility of integrating new data of species, timings and localities, than a species-specific equation for application in real fields. For these reasons and for the different nature and performance of the vegetation indices and structural crop properties, the calibration of global multiple regression models combining various properties for AGB estimation was attempted. Firstly, the calibration of a backward stepwise linear regression model led to the estimation of AGB with $R_{CV}^2 = 0.75$ and nRMSECV = 31% using six predictors. These were Hest and five vegetation indices. Secondly, a combined regression model was built using two predictors only, CIg (before saturation, defined using the fraction cover) and Hest (after saturation). This simple model showed encouraging results with $R_{CV}^2 = 0.65$ and nRMSECV = 36%, suggesting that combining vegetation indices and structural crop variables (such as crop height) could improve the estimation of AGB by overcoming the specificity of vegetation indices. Moreover, its simplicity makes it preferable to other complex models for application in real conditions. Nonetheless, the integration of vegetation indices, crop height and fraction cover should be studied over a wider range of aboveground biomass levels, crop species and vegetation indices to produce a robust approach for the estimation of aboveground biomass.

Supplementary Information The online version contains supplementary material available at https://doi.org/10.1007/s11119-022-09960-w.

Acknowledgements The experiment was part of the CoCrop project (CUP E86G16002800007), funded by the European Agricultural Fund for Rural Development (EAFRD) under Measure 16, Operation 16.2.01, of the Rural Development Program 2014-2020 of the Lombardy Region (Italy). The authors thank the students and collaborators who helped in field work and sampling campaigns: Fabio Introzzi, Roberto Fuccella, Riccardo Asti, Matteo Bosso, Federico Concas, Michele Croci, Stefano Virgadaula, Davide Mapelli, Paolo Pozzi, Pietro Zarpellon, Riccardo Beretta. Thanks to Virginia Fassa for her help in map visualization.

Data availability The datasets generated during and analysed during the current study are available from the corresponding author on reasonable request.

Declarations

Conflict of interest The authors declare that they have no conflict of interest.

References

Azimi, S., Kaur, T., & Gandhi, T. K. (2021). A deep learning approach to measure stress level in plants due to nitrogen deficiency. *Measurement, 173*, 108650. https://doi.org/10.1016/j.measurement.2020.108650

Bendig, J., Bolten, A., Bennertz, S., Broscheit, J., Eichfuss, S., & Bareth, G. (2014). Estimating biomass of barley using crop surface models (CSMs) derived from UAV-based RGB imaging. *Remote Sensing, 6*, 10395–10412. https://doi.org/10.3390/rs61110395

Bendig, J., Kang, Y., Aasen, H., Bolten, A., Bennertz, S., Broscheit, J., Gnyp, M. L., & Bareth, G. (2015). Combining UAV-based plant height from crop surface models, visible and near infrared vegetation indices for biomass monitoring in barley. *International Journal of Applied Earth Observation and Geoinformation, 39*, 79–87. https://doi.org/10.1016/j.jag.2015.02.012

Calou, V. B., Teixeira, A. D. S., Moreira, L. C., da Rocha Neto, O. C., & da Silva, J. A. (2019). Estimation of maize biomass using unmanned aerial vehicles. *Engenharia Agrícola, 39*, 744–752. https://doi.org/10.1590/1809-4430-eng.agric.v39n6p744-752/2019

Cao, H., Gu, X., Wei, X., Yu, T., & Zhang, H. (2020). Lookup table approach for radiometric calibration of miniaturized multispectral camera mounted on an unmanned aerial vehicle. *Remote Sensing, 12*, 4012. https://doi.org/10.3390/rs12244012

Corti, M., Cavalli, D., Cabassi, G., Gallina, P. M., & Bechini, L. (2018). Does remote and proximal optical sensing successfully estimate maize variables? A review. *European Journal of Agronomy, 99*, 37–50. https://doi.org/10.1016/j.eja.2018.06.008

Corti, M., Gallina, P. M., Cavalli, D., & Cabassi, G. (2017). Hyperspectral imaging of spinach canopy under combined water and nitrogen stress to estimate biomass, water and nitrogen content. *Biosystems Engineering, 158*, 38–50. https://doi.org/10.1016/j.biosystemseng.2017.03.006

Corti, M., Gallina, P. M., Cavalli, D., Ortuani, B., Cabassi, G., Cola, G., Vigoni, A., Degano, L., & Bregaglio, S. (2020). Evaluation of in-season management zones from high-resolution soil and plant sensors. *Agronomy, 10*, 1124. https://doi.org/10.3390/agronomy10081124

Deery, D., JimenezBerni, J., Jones, H., Sirault, X., & Furbank, R. (2014). Proximal remote sensing buggies and potential applications for field-based phenotyping. *Agronomy, 4*, 349–379. https://doi.org/10.3390/agronomy4030349

Farooque, A. A., Chang, Y. K., Zaman, Q. U., Groulx, D., Schumann, A. W., & Esau, T. J. (2013). Performance evaluation of multiple ground based sensors mounted on a commercial wild blueberry harvester to sense plant height, fruit yield and topographic features in real-time. *Computers and Electronics in Agriculture, 91*, 135–144. https://doi.org/10.1016/j.compag.2012.12.006

Freeman, K. W., Girma, K., Arnall, D. B., Mullen, R. W., Martin, K. L., Teal, R. K., & Raun, W. R. (2007). By-plant prediction of corn forage biomass and nitrogen uptake at various growth stages using remote sensing and plant height. *Agronomy Journal, 99*, 530–536. https://doi.org/10.2134/agronj2006.0135

Goel, N. S., & Qin, W. (1994). Influences of canopy architecture on relationships between various vegetation indices and LAI and FPAR: A computer simulation. *Remote Sensing Reviews, 10*, 309–347. https://doi.org/10.1080/02757259409532252

Gu, Y., Wylie, B. K., Howard, D. M., Phuyal, K. P., & Ji, L. (2013). NDVI saturation adjustment: A new approach for improving cropland performance estimates in the Greater Platte River Basin, USA. *Ecological Indicators, 30*, 1–6. https://doi.org/10.1016/j.ecolind.2013.01.041

Haboudane, D., Miller, J. R., Tremblay, N., ZarcoTejada, P. J., & Dextraze, L. (2002). Integrated narrowband vegetation indices for prediction of crop chlorophyll content for application to precision agriculture. *Remote Sensing of Environment, 81*, 416–426. https://doi.org/10.1016/S00344257(02)000184

Huete, A. R., Liu, H., & van Leeuwen, W. J. (1997). The use of vegetation indices in forested regions: Issues of linearity and saturation. *In IEEE International Geoscience and Remote Sensing Symposium Proceedings, 4*, 1966–1968. https://doi.org/10.1109/IGARSS.1997.609169

Jackson, R. D., & Huete, A. R. (1991). Interpreting vegetation indices. *Preventive Veterinary Medicine, 11*, 185. https://doi.org/10.1016/S0167-5877(05)80004-2

Jimenez-Berni, J. A., Deery, D. M., Rozas-Larraondo, P., Condon, A. T. G., Rebetzke, G. J., James, R. A., Bovill, W. D., Furbank, R. T., & Sirault, X. R. R. (2018). High-throughput determination of plant height, ground cover and aboveground biomass in wheat with LiDAR. *Frontiers in Plant Science, 9*, 237. https://doi.org/10.3389/fpls.2018.00237

Kuhn, M., 2021. caret: Classification and Regression Training. R package version 6.0–90. Retrieved October, 2021, from https://CRAN.R-project.org/package=caret

Lumley, T., based on Fortran code by Alan Miller, 2020. leaps: Regression Subset Selection. R package version 3.1. Retrieved January, 2020, from https://CRAN.R-project.org/package=leaps

Madec, S., Baret, F., de Solan, B., Thomas, S., Dutartre, D., Jezequel, S., Hemmerlé, M., Colombeau, G., & Comar, A. (2017). High-throughput phenotyping of plant height: comparing unmanned aerial vehicles and ground LiDAR estimates. *Frontiers in Plant Science, 8*, 2002. https://doi.org/10.3389/fpls.2017.02002

Marshall, M., & Thenkabail, P. (2015). Developing in situ non-destructive estimates of crop biomass to address issues of scale in remote sensing. *Remote Sensing, 7*, 808–835. https://doi.org/10.3390/rs70100808

Muggeo, V. M. (2008). Segmented: An R package to fit regression models with broken-line relationships. *R News, 8*, 20–25.

MuñozHuerta, R., GuevaraGonzalez, R., ContrerasMedina, L., TorresPacheco, I., PradoOlivarez, J., & OcampoVelazquez, R. (2013). A review of methods for sensing the nitrogen status in plants: Advantages, disadvantages and recent advances. *Sensors, 13*, 10823–10843. https://doi.org/10.3390/s130810823

Mutanga, O., & Skidmore, A. K. (2004). Narrow band vegetation indices overcome the saturation problem in biomass estimation. *International Journal of Remote Sensing, 25*, 3999–4014. https://doi.org/10.1080/01431160310001654923

Noh, H., Zhang, Q., Han, S., Shin, B., & Reum, D. (2005). Dynamic calibration and image segmentation methods for multispectral imaging crop nitrogen deficiency sensors. *Transactions American Society of Agricultural Engineers, 48*, 393–401. https://doi.org/10.13031/2013.17933

Otsu, N. (1975). A threshold selection method from gray-level histograms. *Automatica, 11*, 23–27. https://doi.org/10.1109/TSMC.1979.4310076

Pauly, K., 2016. Towards calibrated vegetation indices from UAS-derived orthomosaics. In *Proceedings of the 13th International Conference on Precision Agriculture*. Retrieved August, 2022, from https://www.ispag.org/proceedings/?action=year_abstracts

Pinter, P. J., Jr., Hatfield, J. L., Schepers, J. S., Barnes, E. M., Moran, M. S., Daughtry, C. S., & Upchurch, D. R. (2003). Remote sensing for crop management. *Photogrammetric Engineering & Remote Sensing, 69*, 647–664. https://doi.org/10.14358/PERS.69.6.647

Poley, L. G., & McDermid, G. J. (2020). A systematic review of the factors influencing the estimation of vegetation aboveground biomass using unmanned aerial systems. *Remote Sensing, 12*, 1052. https://doi.org/10.3390/rs12071052

Prabhakara, K., Hively, W. D., & McCarty, G. W. (2015). Evaluating the relationship between biomass, percent groundcover and remote sensing indices across six winter cover crop fields in Maryland, United States. *International Journal of Applied Earth Observation and Geoinformation, 39*, 88–102. https://doi.org/10.1016/j.jag.2015.03.002

QGIS.org, 2020. QGIS Geographic Information System. QGIS Association. Retrieved January, 2020, from http://www.qgis.org

R Core Team. (2019). *R: A language and environment for statistical computing*. Vienna: R Foundation for Statistical Computing.

Rasmussen, J., Ntakos, G., Nielsen, J., Svensgaard, J., Poulsen, R. N., & Christensen, S. (2016). Are vegetation indices derived from consumer-grade cameras mounted on UAVs sufficiently reliable for assessing experimental plots? *European Journal of Agronomy, 74*, 75–92. https://doi.org/10.1016/j.eja.2015.11.026

Revelle W (2020). psych: Procedures for Psychological, Psychometric and Personality Research. Northwestern University, Evanston, Illinois, USA. R package version 2.0.9, Retrieved September, 2021, from https://cran.r-project.org/web/packages/psych/

Roth, L., & Streit, B. (2018). Predicting cover crop biomass by lightweight UAS-based RGB and NIR photography: An applied photogrammetric approach. *Precision Agriculture, 19*, 93–114. https://doi.org/10.1007/s11119-017-9501-1

Sharma, L. K., Bu, H., Franzen, D. W., & Denton, A. (2016). Use of corn height measured with an acoustic sensor improves yield estimation with ground based active optical sensors. *Computers and Electronics in Agriculture, 124*, 254–262. https://doi.org/10.1016/j.compag.2016.04.016

Shrivastava, A., & Gupta, V. B. (2011). Methods for the determination of limit of detection and limit of quantitation of the analytical methods. *Chronicles of Young Scientists, 2*, 21. https://doi.org/10.4103/2229-5186.79345

Thenkabail, P. S., Smith, R. B., & De Pauw, E. (2000). Hyperspectral vegetation indices and their relationships with agricultural crop characteristics. *Remote Sensing of Environment, 71*, 158–182. https://doi.org/10.1016/S0034-4257(99)00067-X

Tilly, N., Aasen, H., & Bareth, G. (2015). Fusion of plant height and vegetation indices for the estimation of barley biomass. *Remote Sensing, 7*, 11449–11480.

Vincini, M., Frazzi, E., D'Alessio, P., 2006. Angular dependence of maize and sugar beet VIs from directional CHRIS/Proba data. In *Proceedings of 4th ESA CHRIS PROBA Workshop*, pp. 19–21. Retrieved August, 2022, from https://www.researchgate.net/publication/228413259_Angular_dependence_of_maize_and_sugar_beet_VIs_from_directional_CHRISProba_data

Wang, C., Feng, M. C., Yang, W. D., Ding, G. W., Sun, H., Liang, Z. Y., Xie, Y. K., & Qiao, X. X. (2016). Impact of spectral saturation on leaf area index and aboveground biomass estimation of winter wheat. *Spectroscopy Letters, 49*, 241–248. https://doi.org/10.1080/00387010.2015.1133652

Wickham, H. (2016). *ggplot2: Elegant graphics for data analysis*. Springer-Verlag.

Wiering, N. P., Ehlke, N. J., & Sheaffer, C. C. (2019). Lidar and RGB image analysis to predict hairy vetch biomass in breeding nurseries. *The Plant Phenome Journal, 2*, 190003. https://doi.org/10.2135/tppj2019.02.0003

Authors and Affiliations

Martina Corti[1] · Daniele Cavalli[1,2] · Giovanni Cabassi[2] · Luca Bechini[1] · Nicolò Pricca[2] · Dario Paolo[2,3] · Laura Marinoni[4] · Antonio Vigoni[5] · Luigi Degano[2] · Pietro Marino Gallina[1]

[1] Department of Agricultural and Environmental Sciences-Production, Landscape, Agroenergy, Università degli Studi di Milano, via Celoria 2, 20133 Milano, Italy

[2] Research Centre for Animal Production and Aquaculture, CREA - Council for Agricultural Research and Economics, via Antonio Lombardo 11, 26900 Lodi, Italy

[3] Institute of Agricultural Biology and Biotechnology (IBBA), CNR - Consiglio Nazionale delle Ricerche, Via Edoardo Bassini 15, 20133 Milan, Italy

[4] Research Centre for Engineering and Agro-Food Processing, CREA - Council for Agricultural Research and Economics, via Giacomo Venezian 26, 20133 Milan, Italy

[5] Sport Turf Consulting-Servizi per l'agricoltura con aeromobili a pilotaggio remoto, Via Cesare Battisti, 19, 20027 Rescaldina, MI, Italy